Cell, Vol. 109, 509–521, May 17, 2002, Copyright ©2002 by Cell Press

Antagonism between Ena/VASP Proteins and Actin Filament Capping Regulates Fibroblast Motility

James E. Bear,[1,5] Tatyana M. Svitkina,[2,5] Matthias Krause,[1] Dorothy A. Schafer,[3] Joseph J. Loureiro,[1] Geraldine A. Strasser,[1] Ivan V. Maly,[2] Oleg Y. Chaga,[2] John A. Cooper,[3] Gary G. Borisy,[2] and Frank B. Gertler[1,4]

[1]Massachusetts Institute of Technology
Department of Biology
Cambridge, Massachusetts 02139

[2]Northwestern University School of Medicine
Department of Cell and Molecular Biology
Chicago, Illinois 60611

[3]Washington University School of Medicine
Department of Cell Biology
St. Louis, Missouri 63110

Summary

Cell motility requires lamellipodial protrusion, a process driven by actin polymerization. Ena/VASP proteins accumulate in protruding lamellipodia and promote the rapid actin-driven motility of the pathogen *Listeria*. In contrast, Ena/VASP negatively regulate cell translocation. To resolve this paradox, we analyzed the function of Ena/VASP during lamellipodial protrusion. Ena/VASP-deficient lamellipodia protruded slower but more persistently, consistent with their increased cell translocation rates. Actin networks in Ena/VASP-deficient lamellipodia contained shorter, more highly branched filaments compared to controls. Lamellipodia with excess Ena/VASP contained longer, less branched filaments. In vitro, Ena/VASP promoted actin filament elongation by interacting with barbed ends, shielding them from capping protein. We conclude that Ena/VASP regulates cell motility by controlling the geometry of actin filament networks within lamellipodia.

Introduction

Extension of lamellipodia during cell movement depends upon forces produced by actin assembly (Borisy and Svitkina, 2000; Pantaloni et al., 2001; Pollard et al., 2000). Actin filaments are organized in a dendritic network within protruding lamellipodia, with their barbed, rapidly growing ends oriented toward the membrane (Small et al., 1978). Free barbed ends are created by de novo nucleation or by severing of existing filaments and elongation until capped by capping proteins.

The Ena/VASP protein family has been implicated in lamellipodial dynamics and cell motility (Bear et al., 2000; Rottner et al., 1999). This family consists of the vertebrate proteins Mena, EVL, and VASP and *Drosophila* Ena (Gertler et al., 1996). All share a conserved domain structure that includes the N-terminal EVH1 (Ena/VASP homology) domain and the C-terminal EVH2 domain. The EVH1 domain binds to proteins containing the consensus sequence D/E FPPPPXD/E (abbreviated as "FPPPP") that recruit Ena/VASP proteins to focal complexes and adhesions (Niebuhr et al., 1997) but not to the leading edge (Bear et al., 2000). The EVH2 domain has regions implicated in G and F actin binding and contains a predicted coiled-coil region that mediates oligomerization (Bachmann et al., 1999; Carl et al., 1999). Under certain conditions in vitro, Ena/VASP proteins can nucleate actin polymerization (Huttelmaier et al., 1999; Lambrechts et al., 2000); however, clustering of endogenous Ena/VASP proteins within intact living cells fails to nucleate or recruit new filaments at those sites (Bear et al., 2000; Lasa et al., 1997; Pistor et al., 1994; Skoble et al., 2001).

Regardless of the mechanism, Ena/VASP proteins are implicated in a number of actin-based cellular processes including axon guidance, platelet shape change, and Jurkat T cell polarization (reviewed in Bear et al., 2001). In fibroblasts, Ena/VASP proteins are most highly concentrated in focal adhesions, the leading edge of lamellipodia, and at the tips of filopodia (Gertler et al., 1996; Reinhard et al., 1992). Lamellipodial protrusion rate has been directly correlated with the accumulation of Ena/VASP proteins at leading edges, suggesting that Ena/VASP proteins promote leading edge protrusion (Rottner et al., 1999). In addition, Ena/VASP proteins are required for full motility of the actin-dependent intracellular pathogen *Listeria monocytogenes* (reviewed in Cameron et al., 2000).

Paradoxically, fibroblasts lacking all endogenous Ena/VASP proteins (MV^{D7} cells) translocated faster than derivative cells that reexpress Mena (Bear et al., 2000). To confirm this observation in another cell type, the specific, high-affinity interaction between the EVH1 domains and the FPPPP ligand was used to sequester Ena/VASP proteins within Rat2 cells (Bear et al., 2000). Cells in which all Ena/VASP proteins were sequestered on the mitochondrial surface ("FPPPP-Mito cells") moved faster than control cells. When the relocalization strategy was modified to recruit Ena/VASP proteins to the membrane ("FPPPP-CAAX cells"), we observed a reduction in translocation speed. Together, these results indicate that Ena/VASP proteins reduce fibroblast translocation rates when localized to the plasma membrane.

How can these apparently paradoxical observations about Ena/VASP proteins be reconciled? Since net cell translocation is an integration of cell behavior over many cycles of lamellipodial protrusion and withdrawal, we analyzed the protrusive component of cell motility and determined the supramolecular consequences of manipulating Ena/VASP function in lamellipodia. We present data indicating that Ena/VASP proteins regulate actin network geometry and thereby control protrusive behavior. At a molecular level, Ena/VASP proteins interact directly with the barbed ends of actin filaments at the leading edge, shielding them from the activity of capping protein while supporting filament elongation.

[4]Correspondence: fgertler@mit.edu

[5]These authors contributed equally to this work.

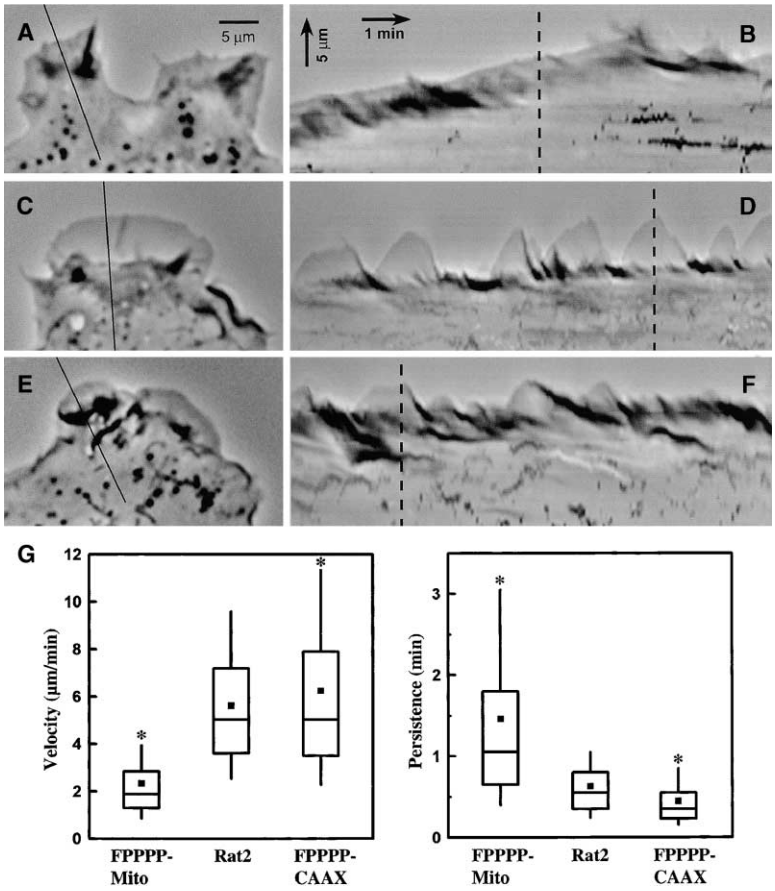

Figure 1. Kymograph Analysis of Rat2, FPPPP-Mito, and FPPPP-CAAX Cells

(A–F) Individual frames (A, C, and E) and kymographs (B, D, and F) from time-lapse movies of FPPPP-Mito (A and B), Rat2 (C and D), and FPPPP-CAAX (E and F) cells. Kymographs show lamellipodial activity along the lines in respective phase contrast images. Ascending and descending contours of the edge indicate protrusion and withdrawal events, respectively, steeper angles of the slopes corresponding to higher rates. Dark shades during withdrawal events correspond to ruffles. Dashed lines on kymographs indicate positions of shown frames in the time-lapse sequences. Scale bar for (A), (C), and (E) and scale vectors for (B), (D), and (F) are shown in top images.

(G) Box and whisker plots for velocity and persistence of individual events of protrusion for FPPPP-Mito, Rat2, and FPPPP-CAAX cells. Dot indicates mean, middle line of box indicates median, top of box indicates 75th quartile, bottom of box indicates 25th quartile, and whiskers indicate extent of 10th and 90th percentiles, respectively. Data for FPPPP-Mito comes from 814 events of protrusion in 42 cells; for Rat2, from 1,399 events of protrusion in 67 cells; and for FPPPP-CAAX, from 1,010 events of protrusion in 29 cells. ANOVA $p < 0.0001$ for both velocity and persistence. Nonoverlapping 95% confidence intervals indicated by asterisks.

Results

Ena/VASP Proteins Regulate Lamellipodial Dynamics and Actin Network Architecture

We analyzed the role of Ena/VASP proteins during lamellipodial protrusion kinetically and structurally. For kinetic analysis, we employed kymography (Hinz et al., 1999). A kymograph is a montage created by extracting intensity values along a defined line region in each image of a time-lapse series and pasting them side-by-side to generate a composite image of object movement over time. In our analysis, we used a 1-pixel-wide line drawn in the direction of cell protrusion. The resulting kymographs reveal the dynamics of membrane activity at a single point along the cell perimeter. Analysis of such kymographs permits quantification of membrane extension rates and determination of the average time the membrane is engaged in individual protrusions.

Kymographs of normal fibroblasts such as Rat2 cells appeared as a series of "shark fin"-like structures reflecting cycles of protrusion and withdrawal (Figures 1C and 1D). In contrast, kymographs of FPPPP-Mito cells appeared as "dunes," reflecting protrusions that extend slowly over time and rarely withdraw (Figures 1A and 1B). Lamellipodia of FPPPP-Mito cells protruded at a lower velocity, but persisted significantly longer than controls (Figure 1G). Over time, this behavior results in more net membrane extension in FPPPP-Mito cells than in control cells, consistent with the increased cell shape change reported previously (Bear et al., 2000). Kymographs of FPPPP-CAAX cells appeared as "shark teeth" (Figures 1E and 1F), reflecting short protrusions quickly replaced by withdrawals, usually as ruffles that appear as dark shades on the kymographs. Analysis of the FPPPP-CAAX cells revealed a statistically significant increase in protrusion velocity with respect to control cells (Figures 1G and 4E).

To observe nascent lamellipodia, we examined cells recovering from ATP depletion (Svitkina et al., 1986). In the absence of glucose, sodium azide causes a rapid depletion of cellular ATP. Without ATP, actin assembly is impaired, presumably due to a lack of ATP bound actin monomers. Upon washout of sodium azide, actin assembly is restored, and a large, synchronous burst of membrane protrusion occurs. In time-lapse movies of FPPPP-Mito and FPPPP-CAAX cells, we observed striking differences during ATP recovery (Figure 2; see Supplemental Movies at http://www.cell.com/cgi/content/full/109/4/509/DC1). In FPPPP-Mito cells, new lamellipodia were smooth and almost entirely free of phase-dark ruffles (arrow, Figure 2). In contrast, FPPPP-CAAX cells formed protrusions irregular in shape that contained large numbers of ruffles (asterisk, Figure 2). With this treatment, Rat2 control cells showed an intermediate phenotype with some areas of flat lamellipodia and some ruffles (data not shown). Similar results were observed with high concentrations of cytochalasin D applied via micropipette to block actin assembly followed

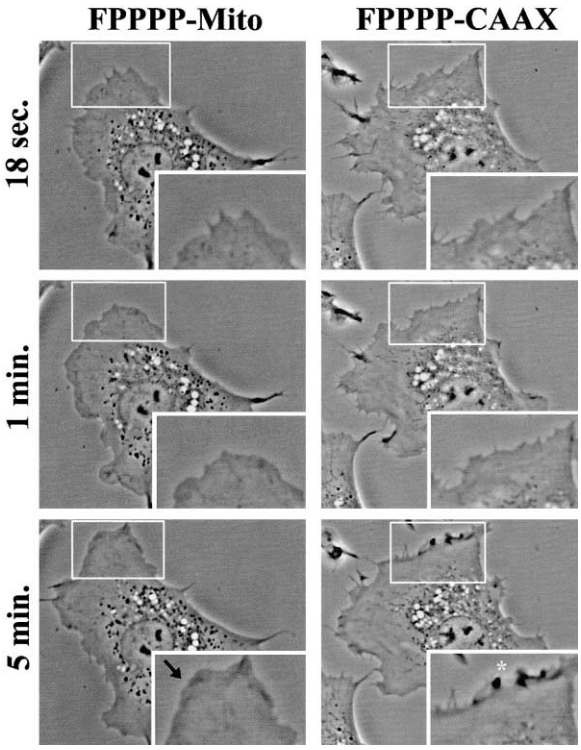

Figure 2. Time-Lapse Analysis of Nascent Lamellipodia

FPPPP-Mito and FPPPP-CAAX cells were filmed during ATP recovery. Panels show individual frames from time-lapse movies (see Supplemental Movies at http://www.cell.com/cgi/content/full/109/4/509/DC1). Labels indicate time after NaN_3 washout/restoration of nutrient media. Insets show 1.5× magnified regions from boxed areas. Black arrow in 5 min inset indicates new lamellipodial protrusion; white asterisk indicates area of ruffling.

by washout (data not shown), suggesting that this effect is not specific for sodium azide treatment.

We reasoned that Ena/VASP-dependent changes in lamellipodial behavior result from altered organization of the underlying actin network. We examined the supramolecular organization of the actin filament network in nascent and mature lamellipodia by platinum replica electron microscopy. Striking differences were observed 1 min after recovery from ATP depletion. Compared to control cells, FPPPP-Mito cells appeared to have shorter and more highly branched filaments (Figure 3A). In contrast, FPPPP-CAAX cells displayed strikingly longer and more sparsely branched actin filaments (Figure 3A). Additional differences in actin network organization were observed 3 min after recovery (Figure 3A). At this time point, actin filaments in control cells appeared longer and were organized in a normal diagonal array, whereas the filaments in FPPPP-Mito cells appeared short and highly branched (Figure 3A). In contrast, the longer filaments in FPPPP-CAAX cells appeared to become oriented predominantly parallel to the plasma membrane (Figure 3A).

Mature lamellipodia of cells engaged in normal translocation displayed similar changes in filament organization. Compared to the diagonal network of actin filaments in control cells, FPPPP-CAAX cells had filaments running predominantly parallel to the leading edge (Figure 4C). FPPPP-Mito cells had a diagonal network of short filaments immediately next to the leading edge, but deeper within lamellipodia (>0.3–0.5 μm), filaments were predominantly oriented perpendicular to the leading edge (Figure 4C). To confirm that differences in actin architecture observed in Rat2 cells with altered distribution of Ena/VASP proteins are not cell type specific, we examined the actin network of MV^{D7} cells (lacking all Ena/VASP proteins) and compared them to a rescued derivative. For both nascent and mature lamellipodia, similar differences were seen in these two lines (see Supplemental Figures S1 and S2 at http://www.cell.com/cgi/content/full/109/4/509/DC1). In addition, Rat2 cells overexpressing Mena showed similar phenotypes to FPPPP-CAAX cells.

To quantify changes in structural features of the actin network in the different cell types, we measured filament length, branching frequency, and orientation at the leading edge. To determine length and branching, we utilized cells recovering from ATP depletion, since under these conditions cells have synchronized, uniformly protruding lamellipodia that permit better visualization of actin filaments. Confirming the visual impression, FPPPP-Mito cells had shorter filaments that branched more frequently than controls (Figures 3B and 3C). Conversely, FPPPP-CAAX cells had longer filaments that branched less frequently (Figures 3B and 3C). In mature lamellipodia, the high filament density made it impossible to directly measure individual filament length and branching frequency. Therefore, for these lamellipodia, we evaluated changes in filament orientation. Changes in filament orientation arise, at least in part, as a consequence of changes in filament length and branching. To quantify filament orientation, we applied the Radon transformation method, recently used to evaluate the lamellipodia of cells engaged in normal translocation (Maly and Borisy, 2001). This method uses a computer algorithm to extract the angles at which actin filaments within lamellipodia approach the plasma membrane ("angle of incidence"). A value of 0° indicates that the filament runs in the direction of protrusion. Quantification by this approach confirmed that FPPPP-CAAX cells had significantly more filaments with greater angles of incidence than control cells, while FPPPP-Mito cells had more filaments with smaller angles of incidence than control cells (Figure 4D; see Supplemental Figure S3 at http://www.cell.com/cgi/content/full/109/4/509/DC1).

Cell Translocation Rates and Lamellipodial Dynamics Are Linked to Actin Network Architecture

Our results show that Ena/VASP deficiency leads to shorter actin filaments, more persistent lamellipodial protrusion, and faster net cell translocation (Bear et al., 2000). If the major function of Ena/VASP proteins is to control filament length, then treatments that reduce filament length should increase cell speeds. We used cytochalasin D (CD), a fungal metabolite that binds to barbed ends of actin filaments with high affinity (2 nM) (Cooper, 1987), for this purpose. To disrupt the actin cytoskeleton in living cells, CD is often used at concentrations in the range of 1–10 μM. At these concentrations, low-affinity interactions with actin monomers and dimers become a confounding factor in interpreting the specificity of

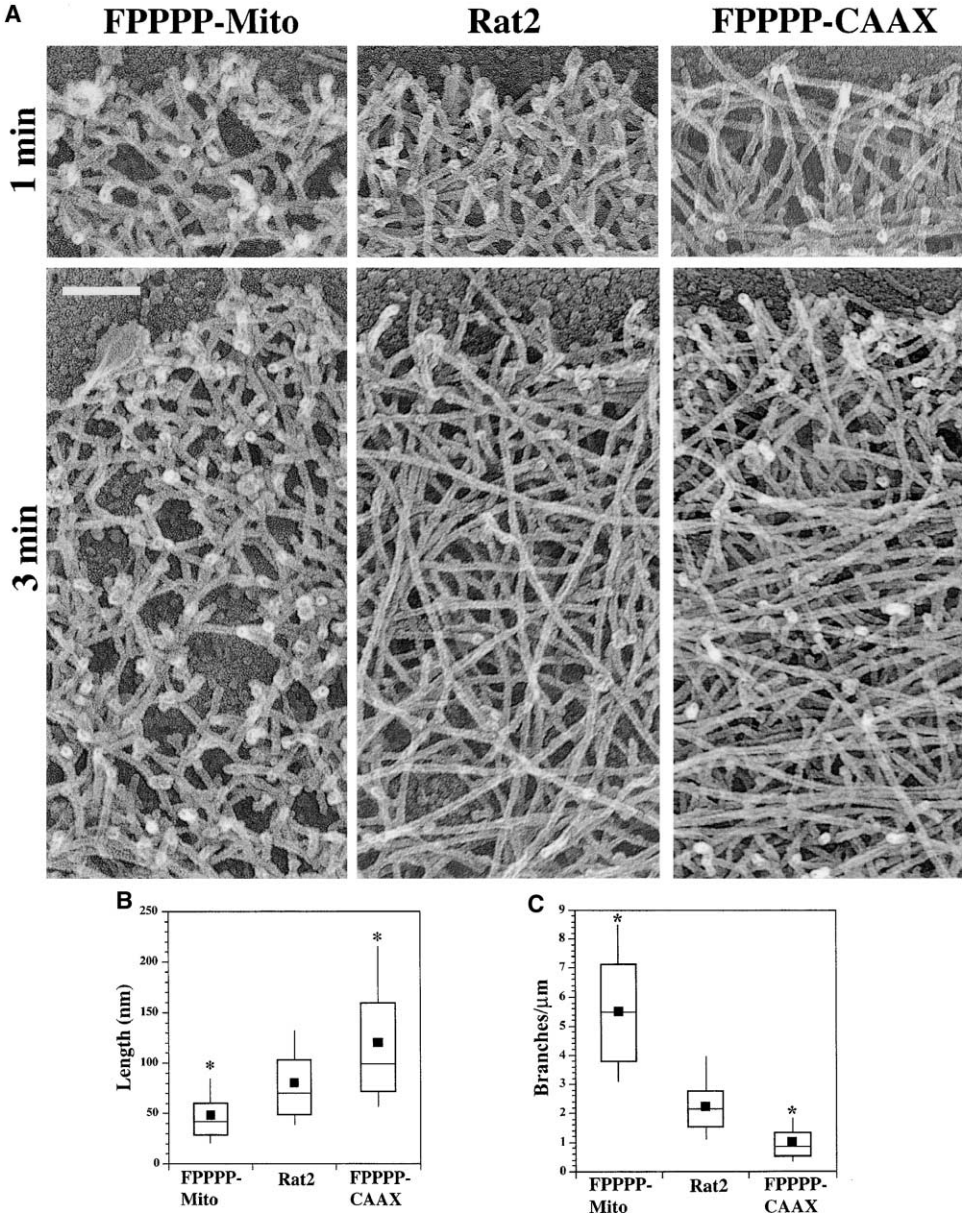

Figure 3. Actin Network Supramolecular Organization upon ATP Recovery

(A) Platinum replica electron microscopy of lamellipodia of FPPPP-Mito, Rat2, and FPPPP-CAAX cells 1 min or 3 min after recovery from ATP depletion. The scale bar equals 100 nm.

(B) Length quantitation. For FPPPP-Mito cells, n = 178 filaments from 25 cells; for Rat2 cells, n = 156 filaments from 16 cells; for FPPPP-CAAX, n = 141 filaments from 14 cells.

(C) Branching frequency. For FPPPP-Mito, n = 26 images from 15 cells; for Rat2 cells, n = 37 images from 13 cells; for FPPPP-CAAX, n = 40 images from 12 cells. For both (B) and (C), ANOVA $p < 0.0001$, nonoverlapping 95% confidence intervals are marked with an asterisk.

the effect. However, at lower doses, CD impairs actin assembly by specifically reducing the rate of actin monomer addition onto barbed ends.

We examined the effects of a range of low CD concentrations on the translocation rate of control Rat2 cells. A biphasic response pattern in cell translocation rate was observed in Rat2 cells (Figure 4A). At 5 nM, cell speed was not increased significantly. At 25 nM, however, cell speed increased significantly. At 50 nM, cell speeds were similar to the untreated controls, while 500 nM CD reduced cell speeds. These results indicate that some barbed end elongation is essential for cell translocation, but that partially limiting this process causes cells to move faster. We next examined the effect of CD treatment on the FPPPP-CAAX and FPPPP-Mito cells. Treatment with 25 nM CD increased the speed of FPPPP-CAAX cells to approximately that of control cells (Figure 4B). This same dose, however, caused FPPPP-Mito cells to slow down (Figure 4B).

In addition to the effects on translocation rate, low-dose CD treatment reversed the effects of Ena/VASP function on actin filament orientation. FPPPP-CAAX

cells treated with 25 nM CD exhibited a reduction of filaments oriented parallel to the edge and contained an increased abundance of filaments oriented diagonally with respect to the edge (Figures 4C and 4D; see Supplemental Figure S3 at http://www.cell.com/cgi/content/full/109/4/509/DC1). The diagonally oriented filaments appeared shorter. CD-treated FPPPP-CAAX cells had a distribution of angles of incidence indistinguishable from untreated Rat2 cells. CD at 25 nM induced a similar shift of Rat2 angles of incidence toward that of untreated FPPPP-Mito cells. No effect of CD on incident angle was observed in FPPPP-Mito cells.

Analysis of lamellipodial dynamics by kymography revealed that treatment with 25 nM CD induced concomitant decreases in protrusion velocity (Figure 4E) and increases in the persistence of protrusions (Figure 4F) in all of the cell types. The greatest effects of CD were observed in the FPPPP-CAAX cells, perhaps because the abnormal filament elongation in these cells was more sensitive to CD than filaments of Rat2 cells or FPPPP-Mito cells. Interestingly, FPPPP-Mito lamellipodia exhibited a slight decrease in protrusion velocity and increase in persistence despite having overall net decrease in translocation speed in 25 nM CD.

To verify that the low dose of CD used in these experiments reduced filament lengths in vivo, we quantified filaments at the leading edge in cells recovering from ATP depletion in the presence or absence of 25 nM CD (Figure 4G). A striking reduction in filament length was observed in the CD-treated FPPPP-CAAX cells, while a smaller but statistically significant decrease was observed in CD-treated Rat2 cells. No effect on length was observed in the FPPPP-Mito cells, perhaps because they already have abnormally short filaments. CD treatment had no effect on the frequency of branching in any of the cell types (data not shown). Taken together, these data indicate that treatment with 25 nM CD decreases filament length in lamellipodia and shifts the translocation rates, orientation of actin filaments, and lamellipodial dynamics of FPPPP-CAAX cells toward those of untreated Rat2 cells, and the properties of Rat2 cells toward those of untreated FPPPP-Mito cells.

Free Barbed Ends of Actin Filaments Are Required to Target Ena/VASP Proteins to the Leading Edge and Filopodial Tips

Ena/VASP proteins are targeted to the leading edge and the tips of filopodia by an unknown mechanism. Since both locations contain high concentrations of free barbed ends of actin filaments, we asked whether the barbed ends themselves might be required to recruit Ena/VASP proteins to these places. In cells, CD effectively masks free barbed ends. We used a range of CD concentrations from 10 nM to 200 nM to determine whether inhibiting barbed end elongation would affect EGFP-Mena localization. These experiments required a CD-insensitive marker for the leading edge. We found that an antibody to N-WASP stains the leading edge robustly and that this distribution was unaffected by any concentration of CD used in this experiment. In control cells, there was extensive overlap of EGFP-Mena and N-WASP signal at the leading edge (Figures 5A–5D). However, at CD concentrations as low as 25 nM, the EGFP-Mena signal at the leading edge was reduced relative to N-WASP and F actin (data not shown). Between 100 and 150 nM CD, EGFP-Mena was displaced completely from the leading edge but not from focal adhesions (Figures 6E–6H). At these low concentrations of CD, the actin cytoskeleton showed little visible disruption as assessed by phalloidin staining. Endogenous Mena and VASP showed a similar selective displacement from the leading edge with CD treatment (data not shown). As a specificity control in these experiments, we used latrunculin B (LatB). Unlike CD, LatB interacts with actin monomers and prevents their incorporation into filaments without occluding the free barbed ends. A range of LatB concentrations was tested (10–400 nM). At all concentrations of LatB in which N-WASP was detected at the leading edge ($<$250 nM), EGFP-Mena was still highly colocalized with N-WASP (Figures 5I–5L and data not shown). Therefore, displacement of Ena/VASP proteins from the leading edge by CD is unlikely to result from a general disruption of actin polymerization. Endogenous Mena was also highly concentrated at the tips of filopodia in NG108 neuroblastoma growth cones (Figures 5M–5O). Upon treatment with 100 nM CD, filopodia were still present, but the tip localization of Mena was lost (Figures 5P–5R). LatB treatment had little or no effect on this localization (data not shown). Therefore, the localization of Ena/VASP proteins to fibroblast leading edges and growth cone filopodial tips requires free barbed ends of actin filaments.

The EVH2 Domain, through Its F Actin Binding Motif, Is Required for Leading Edge Targeting

The EVH1 domain is sufficient to target EGFP weakly to the leading edge, along with focal adhesions (Bear et al., 2000). To determine if the EVH1 domain could mediate the free barbed end-based anchoring of full-length Ena/VASP proteins, we treated cells expressing EGFP-EVH1 with doses of CD up to 400 nM and found that, unlike intact Ena/VASP proteins, the weak leading edge signal of EGFP-EVH1 was insensitive to CD treatment (data not shown), indicating that other regions of Ena/VASP proteins are necessary for efficient leading edge targeting of the intact molecules.

Ena/VASP proteins can bind directly to F actin in vitro through an 18-residue motif in the EVH2 domain (Bachmann et al., 1999). We generated an EGFP-tagged form of Mena lacking this motif (MenaΔFAB). Since Ena/VASP proteins oligomerize through a coiled-coil motif within the EVH2 domain, we expressed MenaΔFAB in MV^{D7} cells (lacking all Ena/VASP proteins) to eliminate the possibility that this construct would be targeted indirectly through oligomerization with endogenous Ena/VASP proteins. MenaΔFAB was properly targeted to focal adhesions but was very weak to undetectable at the leading edge (Figure 6), indicating that the F actin binding motif of Ena/VASP proteins is necessary for leading edge targeting of the full-length proteins.

Since the FAB motif within the EVH2 domain was necessary for leading edge targeting, we wondered if the isolated EVH2 domain would be sufficient to mediate targeting to the leading edge. When expressed in MV^{D7}

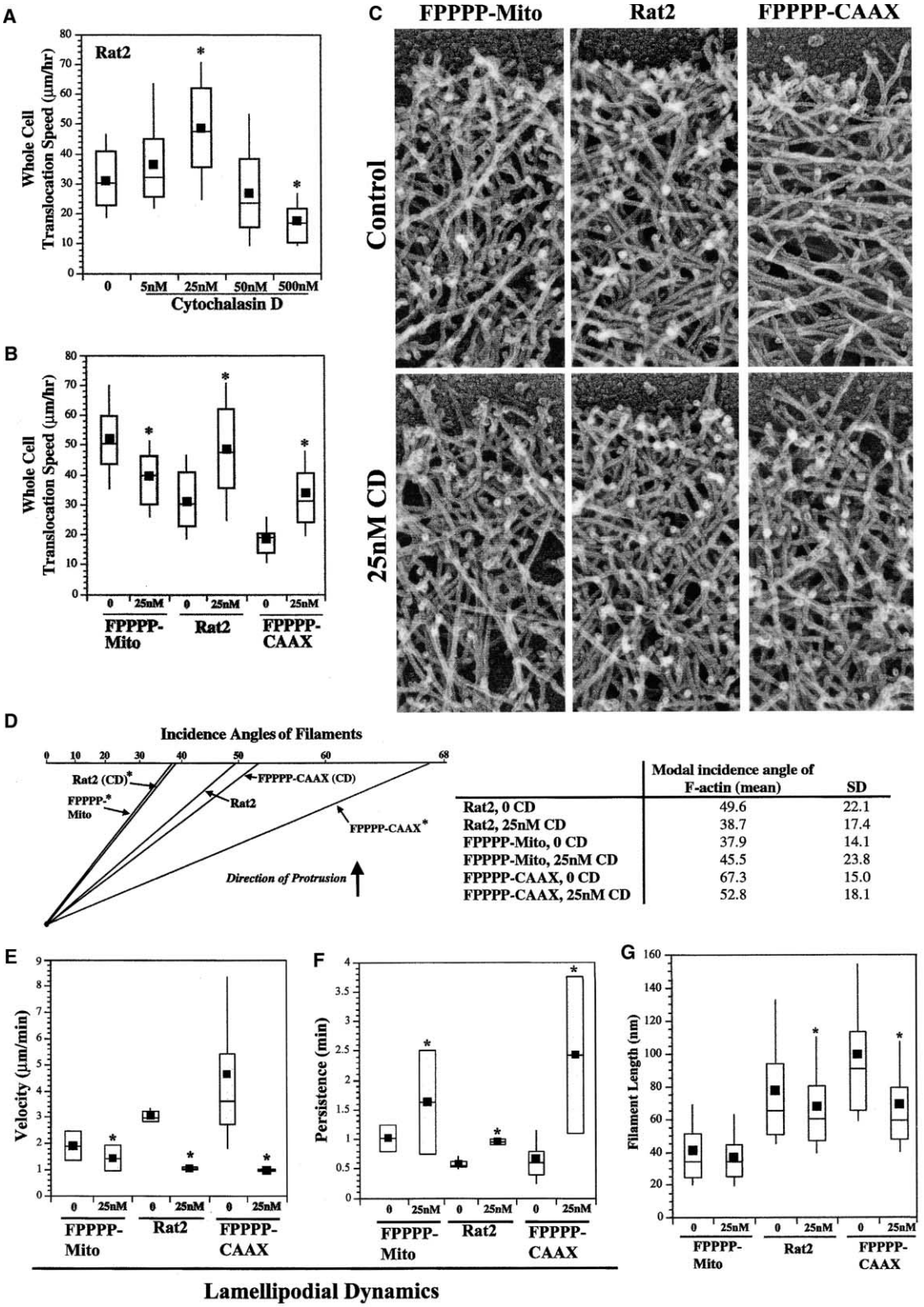

	Modal incidence angle of F-actin (mean)	SD
Rat2, 0 CD	49.6	22.1
Rat2, 25nM CD	38.7	17.4
FPPPP-Mito, 0 CD	37.9	14.1
FPPPP-Mito, 25nM CD	45.5	23.8
FPPPP-CAAX, 0 CD	67.3	15.0
FPPPP-CAAX, 25nM CD	52.8	18.1

Figure 4. Low Dose of Cytochalasin D Counteracts Ena/VASP Activity in Cell Motility

(A) Dose-response curve for cytochalasin D on Rat2 whole-cell speed.

(B) Effect of 25 nM CD on FPPPP-Mito, Rat2, and FPPPP-CAAX whole-cell speed. Data come from two independent experiments. ANOVA $p < 0.0001$ for both experiments. Nonoverlapping 95% confidence intervals are marked by asterisks. Asterisks in (A) reflect differences from untreated control. Asterisks in (B) reflect differences from untreated cognate cell lines.

(C) Platinum replica electron microscopy of control or 25 nM CD-treated cells.

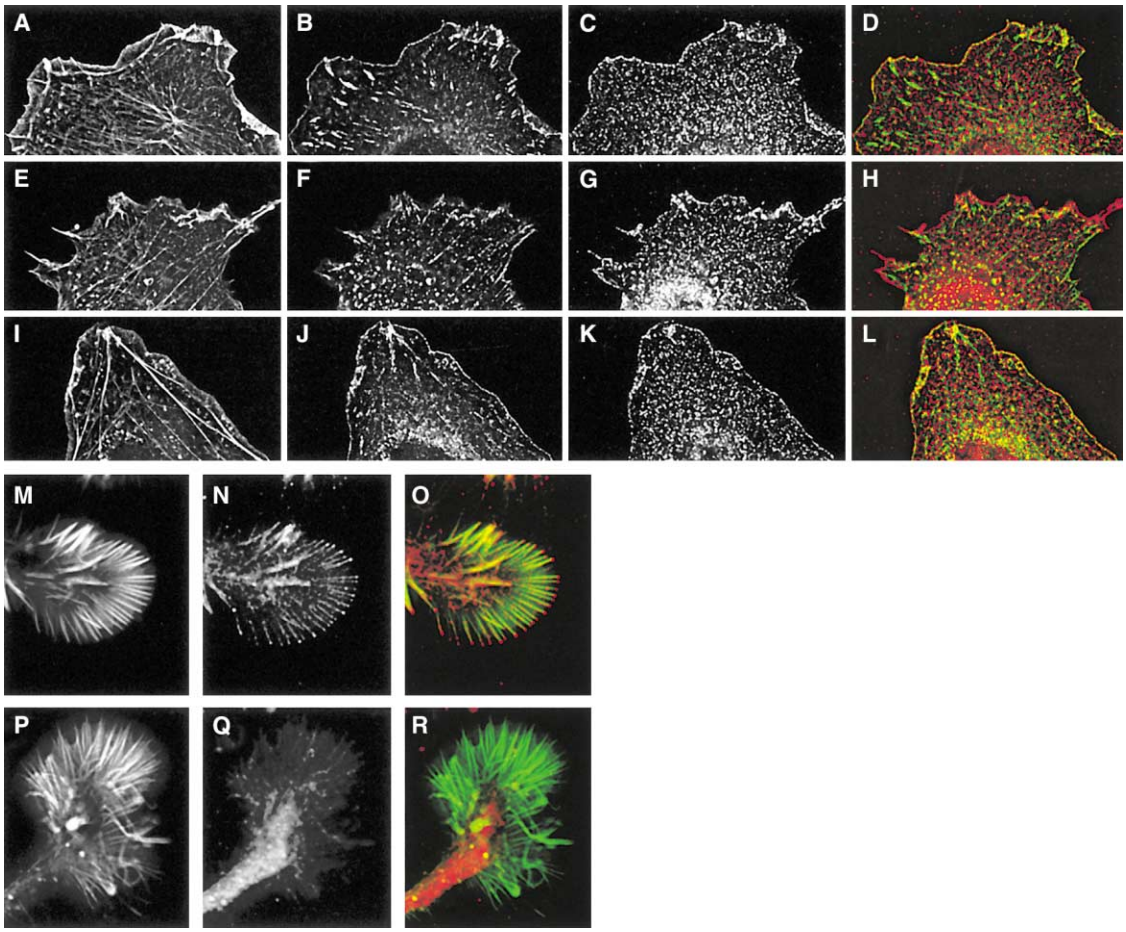

Figure 5. Effect of Cytochalasin D on Ena/VASP Localization at the Leading Edge in Fibroblasts and Filopodial Tips in Growth Cones

(A–L) Immunofluorescence of Rat2 fibroblasts expressing low levels of EGFP-Mena. Control treatment (A–D); 150 nM cytochalasin D, 30 min (E–H); 100 nM latrunculin B, 30 min (I–L). F actin (A, E, and I), EGFP-Mena (B, F, and J), N-WASP (C, G, and K); merge, EGFP-Mena in green, N-WASP in red (D, H, and L).

(M–R) Immunofluorescence of NG108 growth cones. Control treatment (M–O); 100 nM CD, 1 min (P–R). F actin (M and P), Mena (N and Q); merge, EGFP-Mena in green, F actin in red (O and R).

cells, EGFP-EVH2 strongly labeled a broad F actin-rich region throughout lamellipodia but did not decorate focal adhesions or concentrate specifically at the leading edges as does full-length EGFP-Mena (Figure 6; see Supplemental Figures S4 and S5 at http://www.cell.com/cgi/content/full/109/4/509/DC1). The broad region of lamellipodia decorated by EGFP-EVH2 was similar to that seen with Cortactin staining (see Supplemental Figure S4). The localization of EGFP-EVH2 was sensitive to the same doses of CD that displace intact Ena/VASP proteins from the leading edge and filopodial tips (data not shown). When expressed in Rat2 cells, EGFP-EVH2 targeted robustly to the leading edge and focal adhesions (Figure 6). Since this distribution is perfectly coincident with endogenous VASP (data not shown), EVH2 targeting in this cell type was likely due to oligomerization with correctly localized endogenous Ena/VASP proteins. Together, these data indicate that the EVH2 domain is sufficient to target lamellipodia, but that other features such as the EVH1 domain are required to specifically target the leading edge.

VASP-Coated Beads Capture Uncapped But Not Capped Actin Filaments In Vitro

To test whether Ena/VASP proteins bind directly to barbed ends, we utilized an in vitro actin filament capture

(D) Incidence angles of filaments at the leading edge (degrees) as determined by Radon transformation analysis of 18–21 images per treatment. Table contains the mean of the absolute value of the positive and negative modal angles (0° is the direction of protrusion; SD, standard deviations). Asterisks show differences from Rat2 controls (Mann-Witney statistical test; 0.05 cut-off; see Supplemental Figure S3 for more comparisons).

(E) Velocity and (F) persistence of protrusion. ANOVA $p < 0.0001$ for both; nonoverlapping 95% confidence intervals within treatment groups marked by asterisks. Data derived from between 137 and 579 individual events of protrusion per treatment group.

(G) Length of filaments during ATP recovery with or without 25 nM CD. Data come from 164–318 filaments measured per treatment group. ANOVA $p < 0.0001$; nonoverlapping 95% confidence intervals within treatment groups marked by asterisks.

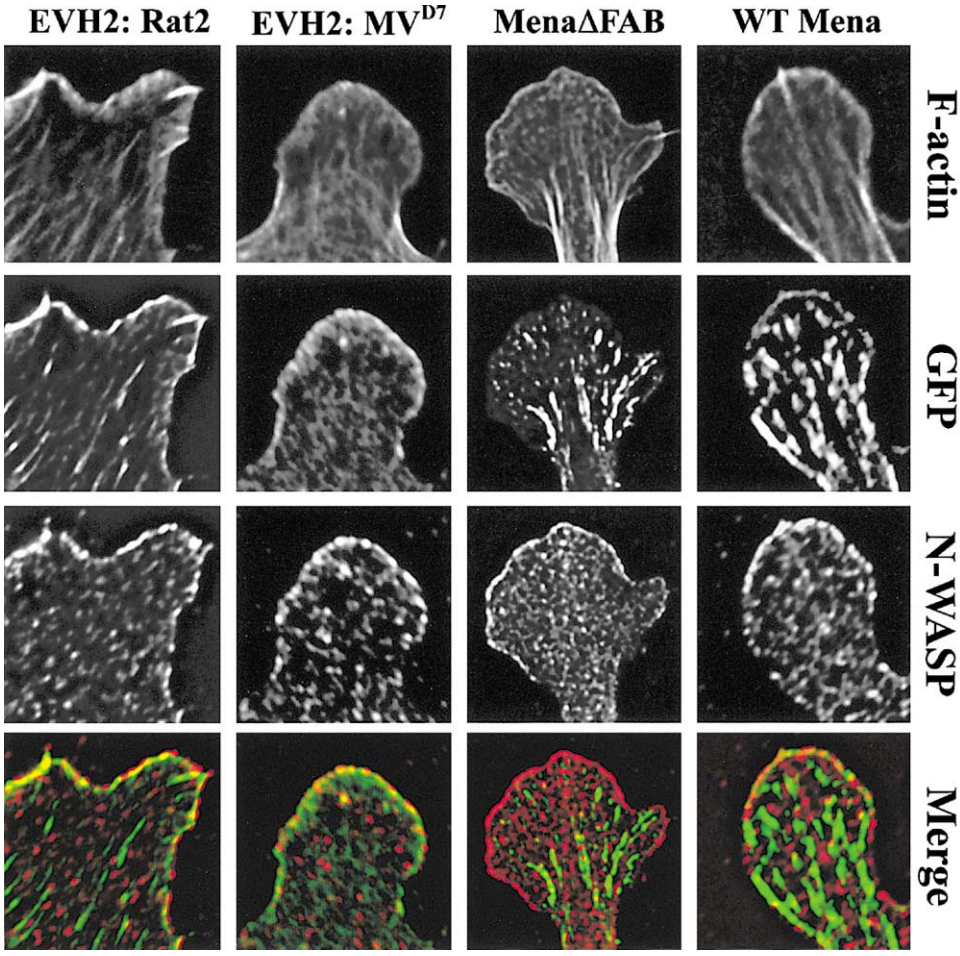

Figure 6. Structural Requirements for Leading Edge Targeting of Ena/VASP Proteins

Immunofluorescence of MV^{D7} or Rat2 fibroblasts expressing full-length EGFP-Mena (wt Mena), EGFP-MenaΔFAB, or EGFP-EVH2. Merge, GFP in green and N-WASP in red.

assay. Protein-coated beads were mixed with actin filaments containing fluorescently-labeled actin monomers (4 μM). To prevent dilution-induced depolymerization during washing, actin filaments were stabilized with phalloidin. Similar results were obtained without phalloidin stabilization, but these experiments were difficult to document due to high background of fluorescence from unattached filaments and unpolymerized monomers (data not shown). Washed bead/filament complexes were examined by fluorescence microscopy.

Beads were coated with a fusion protein containing the FPPPP repeats from ActA. When mixed with fluorescent actin filaments, these FPPPP-alone beads failed to capture filaments (Figure 7A). In contrast, FPPPP beads coated with purified, recombinant VASP (bound to the beads via FPPPP-EVH1 interactions) recruited a high density of actin filaments under the same conditions (Figure 7B). To determine whether the interaction between VASP and actin required free barbed ends, actin filaments were preincubated with either 100 nM or 10 nM purified capping protein (CapZ). Virtually no capture of capped filaments by FPPPP/VASP beads was observed (Figures 7C and 7D). Furthermore, in the absence of F actin, no binding of free CapZ (100 nM) to the FPPPP/VASP beads was detectable (Figure 7G). Once bound to VASP beads, however, uncapped filaments could not be competed off with soluble capping protein (data not shown). To ensure that capping did not depolymerize or otherwise affect the phalloidin-stabilized filaments, we used poly-L-lysine-coated beads as a positive control. The highly charged surface of these beads captures fluorescent actin filaments nonspecifically (Brown and Spudich, 1979). Filament capture was unaffected by preincubating the filaments with 100 nM capping protein (Figures 7E and 7F), indicating that capped filaments were stable under our experimental conditions. From these data we conclude that Ena/VASP proteins likely bind actin filaments directly at or near their barbed ends.

Functional Antagonism between Ena/VASP and Capping Proteins In Vitro

We speculated that Ena/VASP proteins promote filament elongation by interacting with free barbed ends of actin filaments, thereby protecting them from capping protein. To test this hypothesis, we examined the effects of purified VASP on the ability of capping protein to inhibit actin polymerization at barbed ends. Spectrin-F

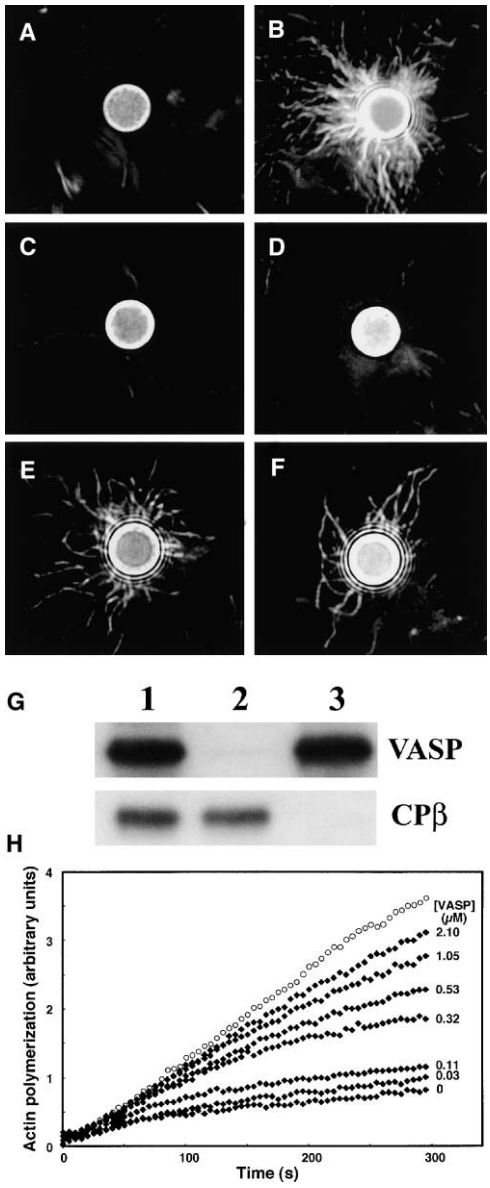

Figure 7. Actin Filament Capture by VASP-Coated Beads and Effects of VASP on Capping Protein during Actin Polymerization

(A–F) In vitro actin filament capture. Paramagnetic beads coated with GST-FPPPP alone do not capture fluorescent actin filaments (A). GST-FPPPP beads bound to VASP capture actin filaments robustly (B). Filaments preincubated with (C) 100 nM or (D) 10 nM capping protein are not captured by GST-FPPPP/VASP beads. Beads coated with poly-L-lysine capture filaments regardless of capping protein preincubation ([E] no capping; [F] 100 nM capping protein). Representative beads are shown; three independent experiments gave identical results.

(G) Pull-down experiment testing for VASP/capping protein interaction: lane 1, starting mixture; lane 2, supernatant; lane 3, washed beads.

(H) VASP inhibits capping by capping protein. Polymerization of 2 μM actin (5% pyrene-labeled) in the absence (open circles) and presence (filled diamonds) of 5 nM capping protein was monitored as the change in pyrene-actin fluorescence versus time. Reactions with capping protein also contained varying concentrations of VASP as indicated to the right of each trace. Actin polymerization was initiated by addition of 0.14 nM spectrin-F actin seeds to the reaction.

actin seeds were used to nucleate polymerization so that filament elongation occurred from barbed ends. We utilized physiological salt concentrations in the assay (100 mM KCl) because these conditions prevent the VASP-dependent nucleation that can be observed in low salt (Huttelmaier et al., 1999). Using these conditions, no effects on elongation kinetics or actin filament nucleation were observed when VASP was added alone (data not shown). Capping protein (CapZ, 5 nM) strongly inhibited elongation (Line labeled "0" in Figure 7H). VASP antagonized the inhibitory effect of capping protein in a dose-dependent manner (Figure 7H). Therefore, Ena/VASP proteins protect actin filaments from the capping activity of capping protein, resulting in increased filament elongation.

Discussion

The Molecular Function(s) of Ena/VASP Proteins

We propose that Ena/VASP proteins interact with actin filaments at or near their barbed ends and prevent or delay binding of capping protein to filaments while permitting continued elongation. Ena/VASP proteins associate with free barbed ends of actin filaments in vitro and, based on CD displacement, free barbed ends are required for leading edge localization of Ena/VASP proteins in vivo. The Ena/VASP-dependent changes in actin filament length in lamellipodia are consistent with VASP's antagonism of capping protein seen by in vitro polymerization assays. In cells, our results suggest that CD treatment largely counteracts the effects of Ena/VASP proteins on cell motility, lamellipodial dynamics, and the architecture of the actin network. Given the known effects of CD on barbed end elongation and our reported effects on filament length in vivo, these observations are consistent with the proposed model for Ena/VASP proteins as "anticapping" proteins. While Ena/VASP proteins may represent the first known proteins with this activity, there may be other proteins with similar functions just as there are multiple types of filament-capping proteins. The inhibition of capping need not be particularly long lasting to produce the observed effects in cells. A transient inhibition of capping would still produce the long filaments observed in the lamellipodia of the FPPPP-CAAX cells. Since the dissociation rate of capping protein from filaments is slow ($t_{1/2}$ = 28 min), capping is essentially a terminal event (Schafer et al., 1996). Ena/VASP proteins may simply slow the association of capping protein with barbed ends.

Our results indicated that Ena/VASP proteins reduced actin filament branching in vivo. Two recent studies using in vitro Arp2/3-induced visual branching assays arrived at different conclusions about the effect of VASP on actin filament branching. One study reported no effect of VASP on branching (Boujemaa-Paterski et al., 2001), while another reported a VASP-dependent inhibition of branching (Skoble et al., 2001). Regardless of how Ena/VASP proteins affect branching, our results from experiments with CD treatment suggest that changes in filament length alone are sufficient to reverse Ena/VASP's effect on cell translocation, lamellipodial dynamics, and filament orientation.

Localization of Ena/VASP Proteins to the Leading Edge

Localization of Ena/VASP proteins to the leading edge involves a combination of both the EVH1 and EVH2 domains. While the EVH1 domain alone was sufficient to target GFP to the leading edge, this targeting was not as robust as the full-length protein and was insensitive to CD treatment (data not shown). The EVH1 domain interacts directly with FPPPP-containing proteins. In the presence of saturating amounts of a cytoplasmic FPPPP construct, Ena/VASP proteins were fully displaced from focal adhesions, but leading edge targeting was indistinguishable from controls (Bear et al., 2000). Importantly, cells expressing the cytoplasmic FPPPP construct exhibited normal translocation speeds, confirming that the remaining leading edge pool of Ena/VASP proteins was functional, and excluded a role for the focal adhesion pool of Ena/VASP proteins in this type of motility assay.

The EVH2 domain also plays a critical role in leading edge targeting. Deletion of the F actin binding motif greatly reduced leading edge targeting but did not affect focal adhesion targeting. The EVH2 domain alone localized to the F actin-rich network within lamellipodia. Unlike full-length Ena/VASP proteins, the EVH2 domain did not become enriched at the leading edge and was undetectable in focal adhesions in Ena/VASP-deficient cells. We propose that leading edge targeting of full-length Ena/VASP proteins requires both the EVH1 and EVH2 domains. The EVH1 domain may act to limit targeting of the EVH2 domain to the very leading edge of the lamellipodium. It is important to point out that different results were observed when the isolated EVH2 domain was expressed in cells containing endogenous Ena/VASP proteins, likely due to oligomerization with endogenous proteins (Bachmann et al., 1999; Huttelmaier et al., 1999; Nakagawa et al., 2001).

Our results suggest that EVH2-dependent recruitment of Ena/VASP proteins to the leading edge requires free barbed ends of actin filaments. Low to moderate doses of CD (100–150 nM), which are expected to cap barbed ends, displaced all Ena/VASP proteins from the leading edges and filopodial tips. This proposed mechanism could explain why Ena/VASP are concentrated at the lamellipodial leading edge in relative proportion to the velocity of protrusion (Rottner et al., 1999). Protruding lamellipodia contain high densities of elongating filaments. As protrusion velocity and free barbed end density increase, greater levels of Ena/VASP proteins would be recruited, thereby changing the architecture of the actin network by increasing filament length and decreasing branching. This would in turn reduce the persistence of the protrusion, providing an adaptive, self-limiting mechanism. Such a mechanism would explain how Ena/VASP proteins could be positive regulators of motility at the local scale (lamellipodia) but negative regulators at the global scale (whole cells). One consequence of decreasing the persistence of protrusion in rapidly extending lamellipodia would be to decrease net cell translocation rates and perhaps increase ruffling. Such behavior might be important for cells to explore their environment and sense guidance cues.

Relationship between Lamellipodial Architecture and Protrusive Behavior

In the absence of Ena/VASP proteins, lamellipodia protruded more slowly but persisted significantly longer than in control cells. In contrast, in cells containing an excess of Ena/VASP proteins at the leading edge, lamellipodial protrusions were faster than in control cells but appeared to be transient and rapidly converted into ruffles. The differences in protrusive behavior correlated with changes in lamellipodial architecture. Within lamellipodia, Ena/VASP proteins increased filament lengths, decreased branching density, and increased angles of incidence. Our results indicate that changes in network geometry alone were sufficient to account for the effect of Ena/VASP proteins on lamellipodial dynamics. How might network geometry be related to protrusive behavior? Mogilner and Oster proposed an "elastic Brownian ratchet" model for lamellipodial protrusion that considers the length and flexibility of actin filaments (Mogilner and Oster, 1996). Transient bending of filaments away from the membrane in the course of thermal fluctuations permits monomer incorporation at the barbed end, and the subsequent restoring force of the bent filament drives membrane protrusion. This model predicts that maximum protrusive force is generated by filaments that have an optimal length of their terminal segment and approach the membrane at an optimal angle. Short filaments are relatively stiff and less able to bend away from the membrane to elongate with new subunits. Long filaments can readily bend and elongate but are not stiff enough to push effectively against the membrane. They will consequently tend to grow and align parallel to the edge. Our observations are consistent with these predictions. Lamellipodia of Ena/VASP-deficient cells contain short, branched (and therefore stiff) filaments and protrude slowly. Although Mogilner and Oster did not explicitly treat withdrawal phases, one may predict that protrusions containing short stiff filaments would tend to be persistent, as we observe. Forces including membrane tension oppose protrusion (Raucher and Sheetz, 2000). Lamellipodia containing long spaghetti-like filaments (resulting from an excess of Ena/VASP activity) may be ineffective in resisting such opposing forces, as evidenced by their tendency to ruffle rapidly.

Relationship between Lamellipodial Protrusion and Cell Translocation

How can changes in local protrusive behavior affect global cell motility? Net cell translocation results from the coordinated activity of four major processes: extension of actin-rich protrusions, such as lamellipodia, stabilization of these protrusions by adhesion to the substratum, translocation of the cell body by contractile forces, and detachment at the rear (Lauffenburger and Horwitz, 1996). There is no simple relationship between the magnitude of any of these parameters and net cell speed. Rather, the optimal combination of these activities plus cell polarization results in productive locomotion. It is important to distinguish between individual events of protrusion and withdrawal and net cell translocation. An individual cycle of protrusion and withdrawal is rapid and brief. In control cells, the leading edge

advances in the protrusive phase at a rate of approximately 5 μm/min and the whole cycle is completed within 1 min. In contrast, net cell translocation rates are measured over several hours with typical values of 0.5 μm/min (30 μm/hr). Thus, net cell translocation reflects an integration of cell behavior over many cycles of protrusion and withdrawal. Biophysical models such as the one of Mogilner and Oster refer specifically to individual protrusive phases, not to net cell translocation. Nevertheless, it is relevant to discuss the extent to which net translocation reflects individual protrusive behavior.

We presented evidence showing a correlation between changes in lamellipodial dynamics and regulation of net cell translocation by Ena/VASP proteins. Our data demonstrate that high instantaneous lamellipodia protrusion rate per se is not sufficient for fast net locomotion. Our results suggest that whole-cell translocation rates are correlated more directly with the persistence of individual protrusions than with their instantaneous velocity. This observation is consistent with work from Hinz and colleagues showing that EGF-stimulated increases in keratinocyte locomotion involved changes in lamellipodia frequency, persistence, and withdrawal but that lamellipodial protrusion velocity remained unchanged (Hinz et al., 1999).

Another factor relevant to lamellipodial dynamics is adhesion to the substratum. We considered whether Ena/VASP proteins' effects on persistence of lamellipodial protrusion might be mediated by adhesion, since VASP has been proposed to play a role in regulating integrin function (Reinhard et al., 2001). We previously showed, however, that in fibroblasts complete depletion of Ena/VASP proteins from focal complexes and focal adhesions had no effect on net cell translocation, provided that the leading edge pool was intact (Bear et al., 2000). Furthermore, the process of membrane protrusion itself does not require adhesion (Bailly et al., 1998). Therefore, it appears unlikely that the effects we have observed on lamellipodial behavior and cell translocation are a direct result of Ena/VASP proteins modulating adhesion receptors. Ena/VASP proteins may indirectly affect adhesion through actin architecture-based changes in lamellipodial behavior. Slow, large, and flat lamellipodia in FPPPP-Mito cells may be more likely to form adhesions with the substratum before the next withdrawal, whereas small and short lamellipodia of FPPPP-CAAX cells with their tendency to form ruffles are less likely to attach efficiently.

In addition to lamellipodial protrusion, other actin-dependent processes such as cell body translocation and cell polarity impact whole-cell translocation rates. Cell body translocation likely depends upon an actin-myosin-based contraction event. Since the efficiency of this contraction depends on the structure of the actin network, it may also be subject to regulation by Ena/VASP proteins. This may explain why CD reduces the whole-cell motility rate of FPPPP-Mito cells while not dramatically altering the filament orientation or lamellipodial dynamics. In addition to effects on cell body translocation, actin plays a role in establishing and maintaining cell polarity. Although we did not investigate cell polarity in detail, we noticed that cells with an excess of Ena/VASP proteins are less polarized than control cells and form protrusions all around the cell perimeter (unpublished observations). Future studies will be directed at understanding these processes and determining how they are integrated with lamellipodial dynamics during whole-cell translocation.

Experimental Procedures

Molecular Cloning and Retroviral Transduction

Subcloning and PCR were performed using standard methods. EGFP-MenaΔFAB is identical to the previously described EGFP-Mena construct except it lacks residues 410–428 (Bear et al., 2000). EGFP-EVH2 is a fusion between EGFP and residues 345–541 of Mena. EGFP-EVH2ΔFAB is identical to EGFP-EVH2 except it lacks residues 410–428. Retroviral packaging, transduction, and FACS sorting were performed as described (Bear et al., 2000).

Cell Culture and Actin-Blocking Drug Treatments

Rat2, MV^{D7}, and derivative cells were cultured as described (Bear et al., 2000). NG108 cells were grown in MEM, 10% fetal calf serum, 1X HAT supplement (GIBCO-BRL). Differentiation was induced by plating cells on poly-L-lysine/Laminin-coated coverslips without serum and with 0.1X HAT supplement (Smalheiser, 1991). Cytochalasin D and latrunculin B (Sigma-Aldrich) were dissolved in DMSO for stock solutions of 3.94 mM and 5 mM, respectively, and stored at −20°C. Drugs were diluted in growth or microscopy media and applied as described in the figure legends.

Kymography and Cell Tracking

For kymography, phase-contrast time-lapse sequences were obtained on a Nikon Eclipse TE200 using a 40× objective. Movies were 10–15 min long with frames taken every 3 s. Kymographs were produced and analyzed using Metamorph software. Kymographs were generated along 1-pixel-wide line regions oriented in the direction of individual protrusions. For quantitative analysis, straight lines were drawn on kymographs from the beginning to the end of individual protrusion events, neglecting fluctuations <0.5 μm (2 pixels) in magnitude. Slopes of these lines were used to calculate the velocities, and projections of these lines along the *x* axis (time) were used to calculate the persistence of protrusions essentially as described (Hinz et al., 1999). Cell tracking movies were made using a 4× phase contrast objective with a frame every 5 min over 2 hr. A minimum of 20 cells from two independent experiments per treatment were analyzed. Data collection and analysis were performed as described (Bear et al., 2000).

ATP Depletion/Recovery Assay

The ATP depletion/recovery assay was performed as described (Svitkina et al., 1986). Cells were adapted to microscopy media for 24 hr and plated on fibronectin-coated ΔT dishes (Bioptechs) as described (Bear et al., 2000). Movies were made using a 40× phase contrast objective with a frame every 3 s. For the time-lapse videomicroscopy experiment, cells were cultured under the standard microscopy conditions described above. To initiate ATP depletion, media was replaced with PBS supplemented with 0.1 g/l $CaCl_2$, 0.1 g/l $MgCl_2$, and 20 mM NaN_3. Cells were incubated for 1 hr. The NaN_3-containing buffer was then replaced with fresh microscopy media to allow ATP recovery. To analyze recovery in the presence of CD, 25 nM CD was added to the azide-containing solution for the last 30 min of starvation and to the washout media.

Platinum Replica Electron Microscopy

For platinum replica electron microscopy, cells on glass coverslips were extracted for 3–5 min with 1% Triton X-100 in PEM buffer (100 mM PIPES-KOH [pH 6.9], 1 mM $MgCl_2$, and 1 mM EGTA) containing 2 μM phalloidin, washed with PEM, fixed with 2% glutaraldehyde in 0.1 M Na-cacodilate (pH 7.3), and processed for electron microscopy as described (Svitkina and Borisy, 1998).

Quantitation of Filament Length, Branching, and Incident Angle

Platinum replica electron micrographs from ATP recovery experiment were coded by number and quantitated blindly. Filament lengths were quantified in a 330 nm high by 660 nm wide image at the leading edge of a lamellipodia by an observer blind to the real identity of the cell using IPLabs software (Scanalytics). The following criteria were applied to filament length measurements: (1) the filament had to have a clearly discernable end oriented approximately toward the leading edge; (2) the filament was traced from the barbed end until it emerged from a mother filament or was lost in the network; and (3) filaments that extended beyond the field of view were excluded. Branching frequency was quantified by counting the number of stereotypical 70° Y-branches in a 330 nm by 330 nm image at the leading edge. To correct for differences in filament density, the number of branches per image was divided by the total length of all visible filaments in the image to derive a normalized branches/μm measurement. To determine the incident angle of F actin, platinum replica electron micrographs of cells undergoing normal translocation were processed by Radon transformation as described (Maly and Borisy, 2001), and the modal incidence angles were extracted from the transformations of individual images.

Immunofluorescence Microscopy

Immunofluorescence microscopy was performed as described (Bear et al., 2000). The N-WASP staining was done with an affinity-purified rabbit polyclonal antibody used at a dilution of 1:1000. This antibody was a kind gift from R. Rohatgi and M. Kirschner. Cortactin staining was done with a mouse monoclonal antibody (4F11, 1:100 dilution; Upstate Biotechnology).

Preparation of Purified VASP and Capping Protein

VASP was purified using the baculovirus system as described (Lambrechts et al., 2000). VASP was stored at 4°C and always used within one month of purification. Mouse capping protein ($\alpha1\beta2$) was expressed, purified, and stored as in Palmgren et al. (2001).

Actin Filament Capture Assay

Paramagnetic polystyrene beads (M-280 tosylactivated Dynabeads, Dynal Biotech) were coated to saturation with GST-FPPPP fusion protein or poly-L-lysine (Sigma-Aldrich) according to the manufacturer's instructions. The GST-FPPPP fusion protein, which consists of GST fused to residues 272–361 from ActA, was expressed using pGEX-2TK and purified from DH5α *E. coli* according to the manufacturer's protocol (Amersham Pharmacia). We mixed 100 μl of a 50% slurry of GST-FPPPP beads with purified VASP (25 μg) in PBS, incubated for 30 min, and then washed three times with F buffer (5 mM Tris-HCl [pH 8], 50 mM KCl, 1 mM $MgCl_2$, 2 mM EGTA, 1% sucrose). Fluorescent actin filaments were polymerized from 4 μM of either Alexa 488-labeled monomers (Molecular Probes) or a 1:4 mixture of labeled:unlabeled monomers (Cytoskeleton) in G buffer (5 mM Tris-HCl [pH 8], 0.2 mM $CaCl_2$, 0.2 mM DTT, 0.2 mM ATP, 10% sucrose) by adding 1/10 volume 10X KME (500 mM KCl, 10 mM $MgCl_2$, 10 mM EGTA, 20 mM Tris-HCl [pH 8]). Identical results were observed with either preparation. Filaments were stabilized with 10 μM phalloidin (Molecular Probes). After phalloidin stabilization, filaments were incubated for 10 min with or without purified capping protein (10 or 100 nM). To test for filament capture, beads were added to filaments and incubated for 10 min. The bead/filament mixture was transferred to a microscope slide resting on a magnet using a wide-bore tip to avoid filament shearing. The beads were held in place for two washes with 100 volumes of F buffer. Washed bead/filament complexes were mounted by adding 25 μl of 37°C low-melting point agarose (0.5% in F buffer) and then positioning a coverslip over the beads. The agarose was allowed to harden at 4°C for 30 min. Samples were documented by fluorescence microscopy using a Deltavision microscope system.

VASP/CapZ Pull-Down Experiment

GST-FPPPP/VASP beads were prepared as described above and mixed with 100 nM capping protein for 30 min in the presence of 4 μM BSA. Beads were separated from supernatant using a magnetic capture stand (Dynal Biotech) and then washed twice with F buffer. Samples of the starting mixture, supernatant, and washed beads were mixed with 5X sample buffer and boiled for 5 min, and equivalent amounts were run on a 10% SDS-PAGE gel. The gel was transferred and processed for Western blotting using standard conditions. VASP was detected with rabbit polyclonal antibody (2010; 1:5000 dilution), and capping protein $\beta2$ subunit was detected by a mouse monoclonal antibody (3F2.3; 1:100 dilution).

Spectrin-F Actin Seeded Actin Polymerization Assay

Spectrin-F actin seeds were prepared from human erythrocytes as described (DiNubile et al., 1995). Actin was purified from chicken pectoral muscle as described (Spudich and Watt, 1971). Pyrene actin was prepared and used as described (Cooper et al., 1983). Actin polymerization from spectrin-F actin seeds was assayed using a final actin concentration of 2 μM containing 0.1 μM pyrene-labeled actin as a tracer for polymerization. Actin assembly was nucleated from spectrin-F actin seeds (0.14 nM) in the presence or absence of 5 nM capping protein and varying amounts of VASP in MKEI buffer (20 mM imidazole [pH 7.0], 100 mM KCl, 2 mM $MgCl_2$, and 1 mM EGTA). Fluorescence of pyrene-actin (excitation at 365 nm and emission at 386 nm) was monitored over 300–600 s at 25°C. The delay between the mixing of reactants and the commencement of fluorescence measurements was less than 10 s.

Acknowledgments

We thank Gretchen Baltus, Amber Murray, and Christy Canida for excellent technical support and Douglas Rubinson for help with statistical analysis. We thank R. Rohatgi and M. Kirschner for the kind gift of the N-WASP antibody. We thank Sally Zigmond, Doug Lauffenburger, and Velia Fowler for helpful suggestions and comments. Work from D.A.S. and J.A.C. was supported by National Institutes of Health grant GM38542 to J.A.C. Work from T.M.S., I.V.M., O.Y.C., and G.G.B. was supported by NIH grant GM62431 to G.G.B. J.J.L. is supported by the Anna Fuller Molecular Oncology Fund. J.E.B. is supported by a Special Fellow award from the Leukemia and Lymphoma Society (3476-02). This work was supported by NIH Glue Grant on Cell Migration IU54 GM63126 (G.G.B. and F.B.G.), by NIH grant GM58801, by funds from Merck & Co., and by the WM Keck Distinguished Young Scholar Award to F.B.G.

Received: August 3, 2001
Revised: April 3, 2002

References

Bachmann, C., Fischer, L., Walter, U., and Reinhard, M. (1999). The EVH2 domain of the vasodilator-stimulated phosphoprotein mediates tetramerization, F-actin binding, and actin bundle formation. J. Biol. Chem. *274*, 23549–23557.

Bailly, M., Yan, L., Whitesides, G.M., Condeelis, J.S., and Segall, J.E. (1998). Regulation of protrusion shape and adhesion to the substratum during chemotactic responses of mammalian carcinoma cells. Exp. Cell Res. *241*, 285–299.

Bear, J.E., Loureiro, J.J., Libova, I., Fassler, R., Wehland, J., and Gertler, F.B. (2000). Negative regulation of fibroblast motility by Ena/VASP proteins. Cell *101*, 717–728.

Bear, J.E., Krause, M., and Gertler, F.B. (2001). Regulating cellular actin assembly. Curr. Opin. Cell Biol. *13*, 158–166.

Borisy, G.G., and Svitkina, T.M. (2000). Actin machinery: pushing the envelope. Curr. Opin. Cell Biol. *12*, 104–112.

Boujemaa-Paterski, R., Gouin, E., Hansen, G., Samarin, S., Le Clainche, C., Didry, D., Dehoux, P., Cossart, P., Kocks, C., Carlier, M.F., and Pantaloni, D. (2001). *Listeria* protein ActA mimics WASp family proteins: it activates filament barbed end branching by Arp2/3 complex. Biochemistry *40*, 11390–11404.

Brown, S.S., and Spudich, J.A. (1979). Nucleation of polar actin filament assembly by a positively charged surface. J. Cell Biol. *80*, 499–504.

Cameron, L.A., Giardini, P.A., Soo, F.S., and Theriot, J.A. (2000). Secrets of actin-based motility revealed by a bacterial pathogen. Nat Rev Mol. Cell. Biol. *1*, 110–119.

Carl, U.D., Pollmann, M., Orr, E., Gertler, F.B., Chakraborty, T., and Wehland, J. (1999). Aromatic and basic residues within the EVH1 domain of VASP specify its interaction with proline-rich ligands. Curr. Biol. *9*, 715–718.

Cooper, J.A. (1987). Effects of cytochalasin and phalloidin on actin. J. Cell Biol. *105*, 1473–1478.

Cooper, J.A., Walker, S.B., and Pollard, T.D. (1983). Pyrene actin: documentation of the validity of a sensitive assay for actin polymerization. J. Muscle Res. Cell Motil. *4*, 253–262.

DiNubile, M.J., Cassimeris, L., Joyce, M., and Zigmond, S.H. (1995). Actin filament barbed-end capping activity in neutrophil lysates: the role of capping protein-beta *2*. Mol. Biol. Cell *6*, 1659–1671.

Gertler, F.B., Niebuhr, K., Reinhard, M., Wehland, J., and Soriano, P. (1996). Mena, a relative of VASP and *Drosophila* Enabled, is implicated in the control of microfilament dynamics. Cell *87*, 227–239.

Hinz, B., Alt, W., Johnen, C., Herzog, V., and Kaiser, H.W. (1999). Quantifying lamella dynamics of cultured cells by SACED, a new computer-assisted motion analysis. Exp. Cell Res. *251*, 234–243.

Huttelmaier, S., Harbeck, B., Steffens, O., Messerschmidt, T., Illenberger, S., and Jockusch, B.M. (1999). Characterization of the actin binding properties of the vasodilator-stimulated phosphoprotein VASP. FEBS Lett. *451*, 68–74.

Lambrechts, A., Kwiatkowski, A.V., Lanier, L.M., Bear, J.E., Vandekerckhove, J., Ampe, C., and Gertler, F.B. (2000). cAMP-dependent protein kinase phosphorylation of EVL, a Mena/VASP relative, regulates its interaction with actin and SH3 domains. J. Biol. Chem. *275*, 36143–36151.

Lasa, I., Gouin, E., Goethals, M., Vancompernolle, K., David, V., Vandekerckhove, J., and Cossart, P. (1997). Identification of two regions in the N-terminal domain of ActA involved in the actin comet tail formation by *Listeria monocytogenes*. EMBO J. *16*, 1531–1540.

Lauffenburger, D.A., and Horwitz, A.F. (1996). Cell migration: a physically integrated molecular process. Cell *84*, 359–369.

Maly, I.V., and Borisy, G.G. (2001). Self-organization of a propulsive actin network as an evolutionary process. Proc. Natl. Acad. Sci. USA *98*, 11324–11329.

Mogilner, A., and Oster, G. (1996). Cell motility driven by actin polymerization. Biophys. J. *71*, 3030–3045.

Nakagawa, H., Miki, H., Ito, M., Ohashi, K., Takenawa, T., and Miyamoto, S. (2001). N-WASP, WAVE and Mena play different roles in the organization of actin cytoskeleton in lamellipodia. J. Cell Sci. *114*, 1555–1565.

Niebuhr, K., Ebel, F., Frank, R., Reinhard, M., Domann, E., Carl, U.D., Walter, U., Gertler, F.B., Wehland, J., and Chakraborty, T. (1997). A novel proline-rich motif present in ActA of *Listeria monocytogenes* and cytoskeletal proteins is the ligand for the EVH1 domain, a protein module present in the Ena/VASP family. EMBO J. *16*, 5433–5444.

Palmgren, S., Ojala, P.J., Wear, M.A., Cooper, J.A., and Lappalainen, P. (2001). Interactions with PIP2, ADP-actin monomers, and capping protein regulate the activity and localization of yeast twinfilin. J. Cell Biol. *155*, 251–260.

Pantaloni, D., Le Clainche, C., and Carlier, M.F. (2001). Mechanism of actin-based motility. Science *292*, 1502–1506.

Pistor, S., Chakraborty, T., Niebuhr, K., Domann, E., and Wehland, J. (1994). The ActA protein of *Listeria monocytogenes* acts as a nucleator inducing reorganization of the actin cytoskeleton. EMBO J. *13*, 758–763.

Pollard, T.D., Blanchoin, L., and Mullins, R.D. (2000). Molecular mechanisms controlling actin filament dynamics in nonmuscle cells. Annu. Rev. Biophys. Biomol. Struct. *29*, 545–576.

Raucher, D., and Sheetz, M.P. (2000). Cell spreading and lamellipodial extension rate is regulated by membrane tension. J. Cell Biol. *148*, 127–136.

Reinhard, M., Halbrugge, M., Scheer, U., Wiegand, C., Jockusch, B.M., and Walter, U. (1992). The 46/50 kDa phosphoprotein VASP purified from human platelets is a novel protein associated with actin filaments and focal contacts. EMBO J. *11*, 2063–2070.

Reinhard, M., Jarchau, T., and Walter, U. (2001). Actin-based motility: stop and go with Ena/VASP proteins. Trends Biochem. Sci. *26*, 243–249.

Rottner, K., Behrendt, B., Small, J.V., and Wehland, J. (1999). VASP dynamics during lamellipodia protrusion. Nat. Cell Biol. *1*, 321–322.

Schafer, D.A., Jennings, P.B., and Cooper, J.A. (1996). Dynamics of capping protein and actin assembly in vitro: uncapping barbed ends by polyphosphoinositides. J. Cell Biol. *135*, 169–179.

Skoble, J., Auerbuch, V., Goley, E.D., Welch, M.D., and Portnoy, D.A. (2001). Pivotal role of VASP in Arp2/3 complex-mediated actin nucleation, actin branch-formation, and *Listeria monocytogenes* motility. J. Cell Biol. *155*, 89–100.

Smalheiser, N.R. (1991). Role of laminin in stimulating rapid-onset neurites in NG108–15 cells: relative contribution of attachment and motility responses. Brain Res. Dev. Brain Res. *62*, 81–89.

Small, J.V., Isenberg, G., and Celis, J.E. (1978). Polarity of actin at the leading edge of cultured cells. Nature *272*, 638–639.

Spudich, J.A., and Watt, S. (1971). The regulation of rabbit skeletal muscle contraction. I. Biochemical studies of the interaction of the tropomyosin-troponin complex with actin and the proteolytic fragments of myosin. J. Biol. Chem. *246*, 4866–4871.

Svitkina, T.M., and Borisy, G.G. (1998). Correlative light and electron microscopy of the cytoskeleton of cultured cells. Methods Enzymol. *298*, 570–592.

Svitkina, T.M., Neyfakh, A.A., Jr., and Bershadsky, A.D. (1986). Actin cytoskeleton of spread fibroblasts appears to assemble at the cell edges. J. Cell Sci. *82*, 235–248.